Materials Science-Poland, 36(2), 2018, pp. 288-296
http://www.materialsscience.pwr.wroc.pl/
DOI: 10.2478/msp-2018-0046

DE GRUYTER OPEN

Gas composition influence on the properties of boron-doped diamond films deposited on the fused silica

BARTŁOMIEJ DEC[1], MATEUSZ FICEK[1,*], MICHAŁ RYCEWICZ[1], ŁUKASZ MACEWICZ[1], MARCIN GNYBA[1], MIROSŁAW SAWCZAK[2], MICHAŁ SOBASZEK[1], ROBERT BOGDANOWICZ[1]

[1]Department of Metrology and Optoelectronics, Faculty of Electronics, Telecommunications and Informatics, Gdansk University of Technology, 11/12 G. Narutowicza St., 80-233 Gdansk, Poland

[2]Polish Academy of Sciences, The Szewalski Institute of Fluid-Flow Machinery, 14 Fiszera St., 80-231 Gdansk, Poland

The main subject of this study are molecular structures and optical properties of boron-doped diamond films with $[B]/[C]_{ppm}$ ratio between 1000 and 10 000, fabricated in two molar ratios of CH_4–H_2 mixture (1 % and 4 %). Boron-doped diamond (BDD) film on the fused silica was presented as a conductive coating for optical and electronic purposes. The scanning electron microscopy images showed homogenous and polycrystalline surface morphology. The Raman spectroscopy confirmed the growth of sp^3 diamond phase and sp^2 carbon phase, both regular and amorphous, on the grain boundaries, as well as the efficiency of boron doping. The sp^3/sp^2 ratio was calculated using the Raman spectra deconvolution method. A high refractive index (in a range of 2.0 to 2.4 at $\lambda = 550$ nm) was achieved for BDD films deposited at 700 °C. The values of extinction coefficient were below 1.4 at $\lambda = 550$ nm, indicating low absorption of the film.

Keywords: *microwave plasma chemical vapor deposition; boron-doped diamond; optical constants; fused silica*

1. Introduction

It has been known for years that diamonds have impressive physical properties including mechanical, thermal [1], electrochemical [2], electronic [3, 4] and biological [5]. A diamond is optically transparent in a range from ultraviolet through visible to the far infrared [6]. This results in multitudinous possibilities of technological applications which include optoelectronic switching devices, optical coatings, wide-band IR optical windows or chemical corrosive operations and high temperature resistance. The diamond has the character of a wide bandgap semiconducting material with $E_g = 5.45$ eV. But when we dope it with boron, it becomes p-type semiconducting material with exceptional electrochemical properties [7]. Boron doped diamond (BDD) film is an excellent electrode material which has a wide electrochemical window, from −1.25 V to 2.3 V in watery electrolytes, compared to a standard hydrogen electrode (SHE) [8] and chemical stability in harsh environments including great biocompatibility [9]. These properties make BDD excellent for use in multitudinous applications including electrochemical sensing [10, 11], biosensing [12, 13], electrocatalysis or wastewater treatment.

For obtaining high-quality diamond thin films, chemical vapor deposition technology is widely used. There are two most common techniques of synthesizing BDD. The first is a hot-filament CVD (HF-CVD), the second is microwave plasma-assisted CVD (MW PA CVD) in-situ doping with boron precursors. The density of boron dopant ranges in MW PA CVD process from 10^{16} atoms per cm^{-3} to 10^{21} atoms per cm^{-3}. P-type semiconducting materials transform into a semimetal with dopant density at 2×10^{20}. Practical applications require optimized structural and morphological properties such as surface smoothness, optical transparency or electrical conductivity. Growth parameters, such as gas mixture, pressure, dopant density or temperature influence in a high degree structure and morphology. Electrical and optical

*E-mail: matficek@pg.edu.pl

properties are also altered with a change in boron dopant density which has been confirmed in the literature [14]. An investigation, conducted by Liao el al. [15], has ended with the conclusion that average grain size of a diamond film decreases up to 10 times with increasing boron density. This effect is caused by re-nucleation which results in smaller crystallite creation on primary larger diamond crystals. Recently, Lu et al. [16] have shown a direct visualization of boron dopant distribution and concluded that boron dopant clearly demonstrates its presence in the diamond lattice connected with enrichment at twin boundaries and defect centers.

Some papers focused on boron doped diamond optical transparent electrodes can be found. Kromka et al. [17] explored the impact of low-temperature MW CVD process on optical properties of nanocrystalline diamond film fabricated on silicon and quartz substrates. The films showed a transmittance of ca. 70 % and high refractive index of 2.34 at 550 nm wavelength. Furthermore, Potocky et al. [18] demonstrated refractive index of 2.2 nm to 2.4 at 550 nm on a quartz substrate grown in a temperature below 400 °C. The optical properties of diamond layers strongly depend on the deposition temperature [19].

Gajewski et al. [20] investigated undoped and low-doped nanocrystalline diamond films deposited on monocrystalline silicon in terms of optical parameters, especially the photocurrent and optical absorption coefficient.

Work carried out by Bennet et al. [21] confirmed increasing influence of boron doping on optical and morphological properties of BDD, suggesting that an area of high conductivity correlates with a high boron doping level along with electrical conductivity heterogeneity of boron-doped poly-/microcrystalline diamond surfaces. The mentioned films have explicit optical properties such as UV-Vis refractive index close to that of undoped and composite NCD films as well as unusual nonzero extinction coefficient due to high boron sub-gap absorption in IR. Boron doping was used to obtain conductive diamond films. In general, the ability to prepare low-resistivity diamond thin films stimulated the present research effort to develop electrochemical and optical applications of this material. The sp^2 carbon could also contribute to the films conductivity. Besides that, the amount of conductive carbon (graphitic, even B containing) at the grain boundaries increases with B addition and supports further charge transport mechanisms. Moreover, B doping produces a material with many different conducting regions, and possibly different conducting pathways and conduction mechanisms [21].

Spectroscopic ellipsometry was performed by Zimmer et al. [22], on heavily doped BDD films for determining their optical properties. An NCD film was deposited on Si wafers at the mean dopant level [B]/[C] of 6500 ppm with the complex index of refraction calculated from the Lorentz model [23].

Nevertheless, there is still a deficiency of information about optical and electrical properties of boron-doped diamond films deposited on transparent substrates in the UV-Vis-NIR region and their spectral dependences. Those critical parameters are crucial for developing integrated sensors [24] or opto-electrochemical bio-sensing devices [25].

In this research, we applied a two-step pretreatment procedure of fused silica substrates to achieve high seeding density and BDD film homogeneity. At first, we used pre-treatment of fused silicon dioxide substrates in hydrogen plasma. Then, the substrates were seeded by spin-coating with PVA mixed with diamond slurry based on diethyl sulfoxide (DMSO) and diamond nanoparticles. The main point of this study were the optical and electrical properties of boron-doped diamond films ($[B]/[C]_{ppm}$ ratio between 5k and 10k) in two molar ratios of CH_4–H_2 mixture (1 % and 4 %). The main motivation for starting this research originated from optimization of growth process parameters of chemical vapor deposition to obtain BDD films with enhanced optical and electrical properties for optical fiber coating [24], opto-electroactive electrodes for energy conversion, optical sensors and spectroelectrochemistry. Thin boron-doped films were deposited by MW PA CVD method on fused silica substrates. Micro-Raman spectroscopy was used to examine molecular structure of the BDD films (sp^3/sp^2 band

ratio) and *ex situ* spectroscopic ellipsometry (SE) was used to measure optical properties, thickness and roughness in UV-Vis-NIR wavelength range. Morphological evaluation was done on the data obtained with scanning electron microscope (SEM).

2. Experimental

The boron-doped diamond films were synthesized in a MW PA CVD system (SEKI Technotron AX5400S). Mirror polished fused silica glass slides (10 mm × 10 mm; 1 mm thick) were used as substrates for experiments. The glass substrates were pre-treated in hydrogen plasma as reported by Bogdanowicz et al. [26]. The seeding process included spinning of thin film from home-made nanodiamond suspension. The detonation nanodiamond (DND) slurry preparation procedure has been reported in the literature [10, 26]. The power of microwaves was kept at 1300 W. Substrate temperature was kept at 700 °C by an induction heater and measured by a thermocouple attached to the backside of a molybdenum substrate stage.

The CH_4–H_2 mixture was kept in this study at 1 % and 4 % of gas volume at 300 sccm of total flow rate. The process pressure was 6.66612 kPa. The doping level of boron in the gas phase, expressed as $[B]/[C]_{ppm}$ ratio, was 1000 ppm, 2500 ppm, 5000 ppm and 10 000 ppm using diborane (B_2H_6) as a dopant precursor (Table 1). A set of undoped diamond films was fabricated for direct boron effect comparison. The growth time was 60 min.

A scanning electron microscope with a tungsten wavelength region source and variable chamber pressure (VP-SEM) was used to inspect the surface of the synthesized thin films. The molecular composition of the films was studied by means of Raman spectroscopy using Raman confocal microscope (InVia, Renishaw, UK). The relative sp^3/sp^2 band ratio was defined from the relation of Raman band areas of: (I) sp^3 diamond lattice line (1332 cm^{-1}), (II) D band assigned to sp^2 phase (1350 cm^{-1}) and (III) G band assigned to distorted sp^2 phase (1520 cm^{-1} to 1600 cm^{-1}).

Spectroscopic ellipsometry investigations were carried out with a phase-modulated ellipsometer Jobin-Yvon UVISEL (HORIBA Jobin-Yvon Inc., Edison, USA). The investigated wavelength region was 250 nm to 800 nm with a step less than 0.5 nm. The experiments were carried out at room temperature using an angle of incidence fixed at 60° and the compensator set at 45°. The incidence angle resulted from Brewster's angle of fused silica substrate. DeltaPsi software (v. 2.4.3) was employed to determine the spectral distributions of refractive index n(λ) and the extinction coefficient k(λ) of the diamond films.

3. Results and discussion

3.1. Surface morphology of boron-doped diamond films

The boron-doped diamond films morphology which were grown on fused silica is presented in Fig. 1. The films were deposited at a temperature of 700 °C at different methane concentrations and [B]/[C] ratios in plasma. Highly crystalline diamond films were obtained for 1k and 5k [B]/[C] ratio for both methane concentrations (1 % or 4 %).

The growth rates of the films were estimated by ellipsometry and are listed in the Table 1. The obvious increase of growth rates of the diamond films was observed for the higher methane admixtures. In contrast, the higher boron concentration in the plasma provided slowdown of diamond growth kinetics. Furthermore, the higher doping level promoted a decrease of average grain size, and reduced the roughness of the films as revealed by SEM images. This phenomenon is attributed to sp^2 phase growth induced by boron complexes causing surface re-nucleation processes. Such graphitic sp^2 phases are much more intensively etched by hydrogen rich plasma (ca. factor of 3), what leads to the lower effective growth rates [27].

The obtained films are not fully covered, which can be observed in the image of 1k $[B]/[C]_{ppm}$ ratio. It can be explained by less effective nucleation and substrate surface termination with oxygen with positive zeta potential, suppressing interactions with the nanodiamond slurry [28]. In case

Table 1. A set of samples and the corresponding deposition parameters.

Sample	CH_4 [%]	[B]/[C] ratio [ppm]	Growth rates [nm/min]
BDD1-0k	1	0k	6.4
BDD1-1k	1	1k	7.7
BDD1-5k	1	5k	7.1
BDD1-10k	1	10k	7.1
BDD4-0k	4	0k	12.3
BDD4-1k	4	1k	14.9
BDD4-5k	4	5k	13.7
BDD4-10k	4	10k	11.6

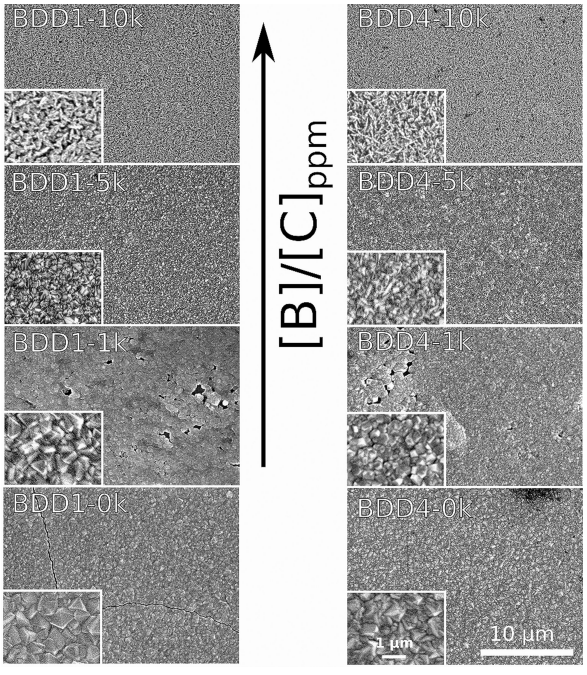

Fig. 1. Scanning electron microscope images of boron-doped diamond films for ($[B]/[C]_{ppm}$ = 0; 1k; 5k; 10k) deposited on fused silica glass at temperature of 700 °C for two different methane concentrations (1 % and 4 %) in the gas mixture.

of 5k $[B]/[C]_{ppm}$ ratio, the polycrystalline, facet-rich morphology was obtained for both methane concentrations. The 5k $[B]/[C]_{ppm}$, films are continuous and fully encapsulated. Furthermore, it is well-known that boron doping influences crystallite size. With increasing boron level in gas phase, the obtained crystallites become smaller. The difference of crystallite sizes is clearly seen in Fig. 1 for 1 % and 4 % methane concentration.

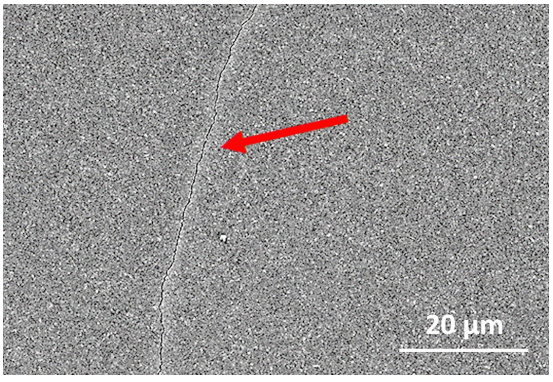

Fig. 2. Scanning electron microscope image of boron-doped diamond film (BDD1-5k) deposited on fused silica. The exposed cracks due to internal stress in the diamond layer can be seen.

In case of $[B]/[C]_{ppm}$ ratio of 10k for both methane ratios, the layers are continuous. However, those layers differ from other samples exhibiting tiny crystallites and significantly higher sp^2 phase contribution as revealed in the Raman spectra (Fig. 3).

It is worth noting that BDD films deposited on fused silica substrates tend to crack due to internal stress in the diamond layer, as illustrated in Fig. 2. It could also be the result of thermal expansion coefficient difference between diamond film and fused silica glass [29].

3.2. Raman spectroscopy

The Raman spectroscopy is a common technique for analyzing different forms of carbon layers. The wide variety of carbon forms arises from

the dependence of their properties on the ratio of sp^2/sp^3. This relation significantly depends on methane concentration in the deposition process. The modification of properties of BDD films, in particular their conductivity, is possible thanks to boron doping.

The Raman spectrum of boron-doped diamond film (in ratio $[B]/[C]_{ppm} = 5k$) deposited on fused silica at 4 % methane concentration is shown in Fig. 3. Decomposition of the peaks was made by Lorentzian function. The values of linewidth (full width at half maximum FWHM) and integral intensity of the peaks in the Raman spectrum of BDD4-5k are listed in Table 2.

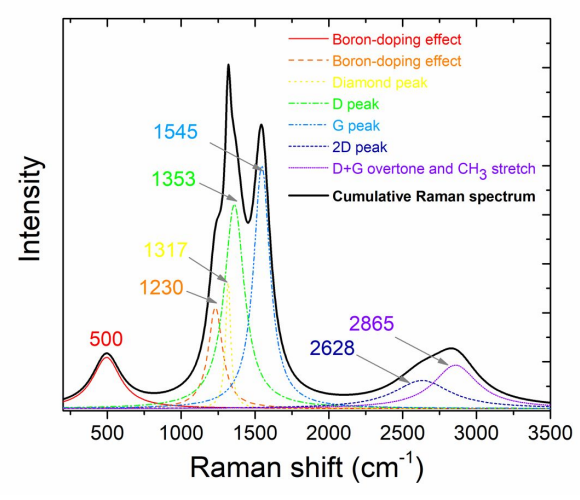

Fig. 3. Normalized Raman spectrum of BDD4-5k ($[B]/[C]_{ppm} = 5k$, obtained at 4 % methane concentration, with peaks decomposition by Lorentzian function.

The Raman spectrum of BDD4-5k consists of a strong narrow line at ~1317 cm^{-1}, which is assigned to sp^3 diamond line corresponding to the vibrations of two interpenetrating cubic sublattices [30]. Due to boron doping, the diamond line has changed its position from its typical position of 1332 cm^{-1} (Fig. 3). This shift is associated with the decrease in the number of pure diamond cells [31, 32].

In the spectrum there are also two characteristic lines around 1360 cm^{-1} and 1550 cm^{-1}, which are attributed to sp^2 carbon. The first one is described as disorder (D), the second as graphite (G). There are also present second order 2D peak around 2600 and D + G overtone ~2850 cm^{-1} [33].

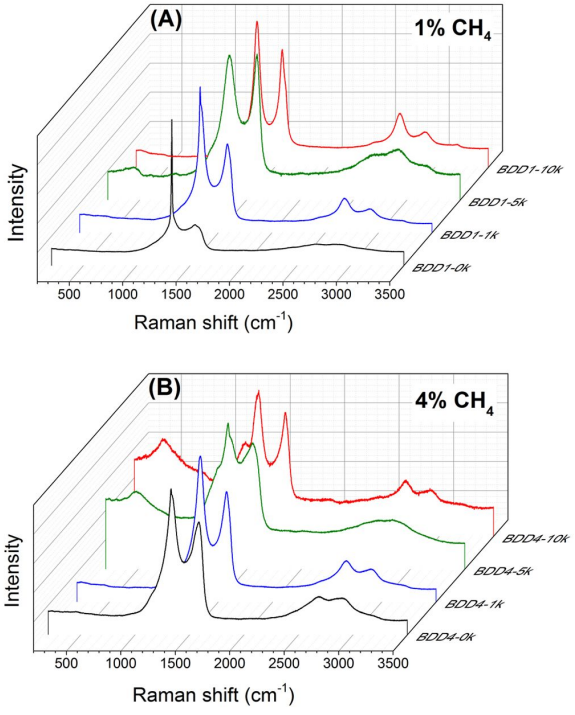

Fig. 4. Raman spectra of boron-doped diamond films ($[B]/[C]_{ppm} = 0k, 1k; 5k; 10k$) deposited on fused silica at temperature of 700 °C at two different methane concentrations ((A) – 1 % and (B) – 4 %). The undoped samples have been shown for comparison.

The effect of boron doping on the diamond lattice can be observed at 1230 cm^{-1} and 500 cm^{-1}. Moreover, these bands have not been observed in the reference undoped samples. Their origin is not obvious, but their position agrees approximately with two maxima in the phonon density of states (PDOS) [34]. The diamond purity of BDD4-5k film was calculated from a relative Raman cross section of diamond to graphite ratio of 1/50 as follows:

$$C_d = 100\, A_d/(A_d + \frac{\sum A_i}{50}) \qquad (1)$$

where A_d and A_i are areas of the fitted curves corresponding to 1317 cm^{-1} diamond peak and

Table 2. Position, integral intensity, full width at half maximum and origin of the peaks in the Raman spectrum of BDD4-5k.

Position [cm^{-1}]	Integral intensity	FWHM [cm^{-1}]	Origin
500	38	232	boron in diamond lattice
1230	38	117	boron in diamond lattice
1317	17	42	diamond peak
1353	108	165	D peak
1545	105	135	G peak
2628	42	466	2D peak
2865	51	367	D + G overtone and CH_3stretching

the graphitic bands, respectively [35]. The estimated diamond purity (C_d) for BDD4-5k was approximately 80.

The Raman spectra of boron-doped carbon films obtained at different methane and boron concentrations in the gas mixture are shown in Fig. 4. Based on the peaks analysis for different methane concentrations, it can be seen that the diamond line decreases and broadens with increasing boron content in the film. The changes in bandwidth are attributed to internal stress in the diamond layer.

The differences in boron concentration (for 4 % methane concentration) can be confirmed by the growth of the bands at 1232 cm^{-1} and around 495 cm^{-1} (Table 3) which is typical of a highly boron doped carbon [36]. Their growth is in good agreement with the shift of position of the Raman band assigned to diamond towards lower values of optical transmission.

Table 3. Integral intensity of the band around 495 cm^{-1} for samples obtained at 4 % methane concentration.

Sample	Integral intensity
BDD4-1k	–
BDD4-5k	38
BDD4-10k	73

In the Raman spectrum of BDD1-1k, one can notice a diamond band around 1332 cm^{-1} from sp^3 phase. This spectrum is a sum of G, D, 2D bands areas, D + G overtone and CH_3 stretch area. The presence of strong 2D peak in some spectra suggests that sp^2 lattice is regular (like in graphene or in nanotubes) contrary to sp^2 amorphous carbon [37]. However, we have not observed significant influence of this feature of molecular composition (regular or irregular sp^2 carbon) on optical properties of the films.

The Raman spectrum of BDD1-5k shows also a mixture of sp^3 and sp^2 carbon phases, but it resembles more sp^2 carbon lattice than sp^3 diamond crystal lattice. It can also be caused by resonant enhancement of Raman signal from sp^2 phase by green laser. A similar composition of diamond phase with strong regular sp^2 can be observed in BDD4-1k. For samples having 10k ppm of boron, the diamond band can be seen only as a weak finger, which confirms disorder caused by boron and presence of sp^2 structure. The spectrum of BDD1-10k consists of crystalline sp^2 and amorphous carbon. Raman spectra analysis confirms the morphologic analysis taken by SEM.

3.3. Optical properties of boron-doped diamond films

In order to extend the optical characterization, the ellipsometry parameters Ψ and Δ were measured for the BDD films. The parameters were obtained at room temperature for 70° angles of incidence in the wavelength of 260 nm to 830 nm. The dispersion of the diamond films was fitted to the Tauc-Lorentz oscillator (TL) model. The fitting process was widely described in our previous work [14]. Subsequently, the estimated optical model was fitted to the experimental data employing the nonlinear Levenberg-Marquardt

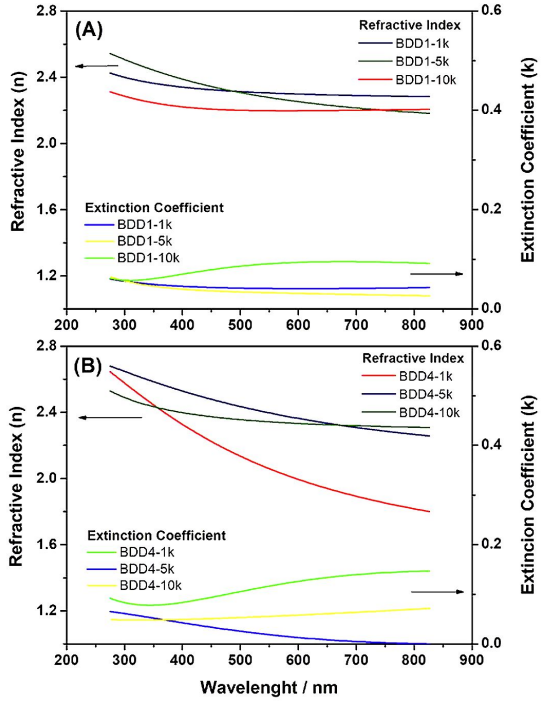

Fig. 5. Variation of optical indices for boron-doped diamond films obtained on fused silica slides at (A) 1 % and (B) 4 % methane admixture and various boron doping levels.

regression method and mean-square error of minimization (MSE) [35]. As a result of the analysis, the refractive index n(λ) and extinction coefficient k(λ) were obtained [36].

Fig. 5 shows spectral variation of n(λ) and k(λ) for diamond films deposited at 1 % and 4 % methane admixture with varied boron concentration in gas phase process at 700 °C during a 60 min process. For all deposited diamond films, the refractive index decreases with increasing wavelength values showing regular dispersion in considered wavelength range. This dependence exhibits usual behavior near the band gap of electronic transition. The only exception is the highly boron-doped diamond, where the n values display a slight shift towards higher wavelengths. The obtained values of the refractive index at $\lambda = 550$ nm are high, varying from 2.19 to 2.30 for BDD films deposited at 1 % methane admixture and from 2.34 to 2.39 at 4 % methane admixture, excluding the heavily doped BDD1-5k film. The decreasing n values are attributed to boron incorporation in the BDD structure, as revealed by Raman studies (Fig. 4). The increased boron doping level stimulates structural imperfections like twin boundaries and planar incoherent defects due to the local boron enrichment [16]. Local structural studies show that these boron rich regions reveal also higher concentrations of non-diamond forms and sp^2 hybridized allotropes [38, 39].

Both increased boron concentration and sp^2 phases increase extinction coefficient, and so intrinsic absorption of the films. The increase of k is attributed to the free carrier absorption (electrons and holes) and could be observed as a near-IR tail (wavelengths $>$ 500 nm). It could be connected with an acceptor level of boron dopant located at 0.38 eV from the top of the valence band as discussed in [40]. Furthermore, the high content of sp^2 phase generally decreases refractive index of the films lowering the density of films, which is partially associated with optical density.

The variation of the extinction coefficient is shown in Fig. 5. The BDD films deposited at 1 % methane concentration reach lower k values than those deposited at 4 %, with all being below 0.09 and 0.11, respectively. It is shown that boron doping with $[B]/[C]_{ppm}$ below 5k results in extinction coefficient below 0.06 which indicates low light absorption. Heavily doped films exhibit an increase in k(λ) values with increasing wavelength, which is abnormal behavior of extinction plot. High extinction coefficient results in limited possible application in optical devices.

4. Conclusions

Summarizing, the boron-doped diamond films were deposited in MW PA CVD process at different methane concentrations and $[B]/[C]_{ppm}$ ratios in plasma, on fused silica glass. Highly crystalline diamond films were obtained for 1k and 5k $[B]/[C]_{ppm}$ ratios at both methane concentrations (1 % or 4 %). It is worth noting that BDD films deposited on fused silica substrates tend to crack due to internal stress in the diamond layer or thermal expansion coefficients difference between

the film and glass substrate. Raman spectroscopy confirmed the presence of diamond sp^3 phase in the deposited films (band at about 1332 cm^{-1}). Thus, the results are generally in good agreement with the results of the SEM analysis. However, only in selected samples these diamond nanocrystals dominate the film structure (e.g. BDD4-5k). The rest of the samples contain both diamond sp^3 crystal and regular sp^2 carbon structures. Moreover, the efficiency of boron doping was confirmed by a shift of Raman line to 1318 cm^{-1} and occurrence of new Raman bands at 495 cm^{-1} and 1231 cm^{-1}, which is in good agreement with optical constants decrease. It is shown that boron doping with $[B]/[C]_{ppm}$ below 5k results in extinction coefficient below 0.06 which indicates a low light absorption required for optical devices.

Acknowledgements

This work was partially supported by the Polish National Science Centre (NCN) under Grant 2016/21/B/ST7/01430 and the National Centre for Research, Development (NCBR) TECHMATSTRATEG1/347324/12/NCBR/2017 and NATO SPS G5147. The DS funds of Faculty of Electronics, Telecommunications and Informatics of the Gdansk University of Technology are also acknowledged.

References

[1] SUKHADOLAU A.V., IVAKIN E.V., RALCHENKO V.G., KHOMICH A.V., VLASOV A.V., POPOVICH A.F., *Diam. Relat. Mater.*, 589 (2005), 3.

[2] INIESTA J., MICHAUD P.A., PANIZZA M., CERISOLA G., ALDAZ A., COMNINELLIS C., *Electrochim. Acta*, 23 (2001), 3573.

[3] ADAMSCHIK M., KUSTERER J., SCHMID P., SCHAD K.B., GROBE D., FLÖTER A., KOHN E., *Diam. Relat. Mater.*, 672 (2002), 3.

[4] PETRŽELA J., VYSKOČIL P., PROKOPEC J., *20th International Conference Radioelektronika 2010*, 4 (2010), 217.

[5] AMARAL M., DIAS A.G., GOMES P.S., LOPES M.A., SILVA R.F., SANTOS J.D., FERNANDES M.H., *J. Biomed. Mater. Res. A*, 1 (2008), 91.

[6] SOBASZEK M., SKOWROŃSKI Ł., BOGDANOWICZ R., SIUZDAK K., CIROCKA A., ZIĘBA P., GNYBA M., NAPARTY M., GOŁUŃSKI Ł., PŁOTKA P., *Opt. Mater.*, 42 (2015), 24.

[7] WORT C.J.H., BALMER R.S., *Mater. Today*, 22 (2008), 1.

[8] BOGDANOWICZ R., CZUPRYNIAK J., GNYBA M., RYL J., OSSOWSKI T., SOBASZEK M., SIEDLECKA E.M., DAROWICKI K., *Sens. Actuat. B-Chem.*, 189 (2013), 30.

[9] WĄSOWICZ M., FICEK M., WRÓBEL M.S., CHAKRABORTY R., FIXLER D., WIERZBA P., JĘDRZEJEWSKA-SZCZERSKA M., *Materials*, 4 (2017), 352.

[10] BOGDANOWICZ R., SOBASZEK M., FICEK M., GNYBA M., RYL J., SIUZDAK K., BOCK W.J., SMIETANA M., *J. Opt. Soc. Korea*, 6 (2015), 705.

[11] KOWALSKA M., FABISIAK K., WRZYSZCZYŃSKI A., BANASZAK A., SZYBOWICZ M., PAPROCKI K., BAŁA W., BYLICKI F., *Mater. Sci.-Poland*, 3 (2014), 475.

[12] MILEWSKA D., KARPIENKO K., JĘDRZEJEWSKA-SZCZERSKA M., *Diam. Relat. Mater.*, 64 (2016), 169.

[13] JĘDRZEJEWSKA-SZCZERSKA M., KARPIENKO K., WRÓBEL M.S., TUCHIN V.V., *Biosensors for Security and Bioterrorism Applications*, Springer International Publishing, 2016.

[14] FICEK M., SOBASZEK M., GNYBA M., RYL J., GOŁUŃSKI Ł., SMIETANA M., JASIŃSKI J., CABAN P., BOGDANOWICZ R., *Appl. Surf. Sci.*, 387 (2016), 846.

[15] LIAO X.Z., ZHANG R.J., LEE C.S., LEE S.T., LAM Y.W., *Diam. Relat. Mater.*, 2 (1997), 521.

[16] LU Y.-G., TURNER S., VERBEECK J., JANSSENS S.D., WAGNER P., HAENEN K., TENDELOO VAN G., *Appl. Phys. Lett.*, 41907 (2012), 4.

[17] KROMKA A., REZEK B., REMES Z., MICHALKA M., LEDINSKY M., ZEMEK J., POTMESIL J., VANECEK M., *Chem. Vap. Depos.*, 181 (2008), 7.

[18] POTOCKY S., KROMKA A., POTMESIL J., REMES Z., VORLICEK V., VANECEK M., MICHALKA M., *Diam. Relat. Mater.*, 744 (2007), 4.

[19] HU Z.G., HESS P., *Appl. Phys. Lett.*, 81903 (2006), 8.

[20] GAJEWSKI W., ACHATZ P., WILLIAMS O.A., HAENEN K., BUSTARRET E., STUTZMANN M., GARRIDO J.A., *Phys. Rev. B*, 45206 (2009), 4.

[21] BENNET K.E., LEE K.H., KRUCHOWSKI J.N., CHANG S.-Y., MARSH M.P., ORSOW VAN A.A., PAEZ A., MANCIU F.S., *Materials*, 5726 (2013), 12.

[22] ZIMMER A., WILLIAMS O.A., HAENEN K., TERRYN H., *Appl. Phys. Lett.*, 131910 (2008), 13.

[23] FICEK M., SANKARAN K.J., RYL J., BOGDANOWICZ R., LIN I.-N., HAENEN K., DAROWICKI K., *Appl. Phys. Lett.*, 241906 (2016), 24.

[24] BOGDANOWICZ R., ŚMIETANA M., GNYBA M., FICEK M., STRAŇÁK V., GOLUŃSKI Ł., SOBASZEK M., RYL J., *Phys. Status Solidi A*, 10 (2013), 1991.

[25] STOTTER J., SHOW Y., WANG S., SWAIN G., *Chem. Mater.*, 19 (2005), 4880.

[26] BOGDANOWICZ R., SOBASZEK M., RYL J., GNYBA M., FICEK M., GOŁUŃSKI Ł., BOCK W.J., ŚMIETANA M., DAROWICKI K., *Diam. Relat. Mater.*, 55 (2015), 52.

[27] BENNET K.E., TOMSHINE J.R., MIN H.-K., MANCIU F.S., MARSH M.P., PAEK S.B., SETTELL M.L., NICOLAI E.N., BLAHA C.D., KOUZANI A.Z., CHANG S.-Y., LEE K.H., *Front. Hum. Neurosci.*, 10 (2016), 102.

[28] HEES J., KRIELE A., WILLIAMS O.A., *Chem. Phys. Lett.*, 12 (2011), 1.
[29] DYCHALSKA A., FABISIAK K., PAPROCKI K., DUDKOWIAK A., SZYBOWICZ M., *Mater. Sci.-Poland*, 620 (2016), 3.
[30] PRAWER S., NEMANICH R.J., *Philos. T. R. Soc. A*, 1824 (2004), 2537.
[31] BRUNET F., GERMI P., PERNET M., DENEUVILLE A., GHEERAERT E., MAMBOU J., *Diam. Relat. Mater.*, 6 (1997), 774.
[32] KRIVCHENKO V.A., LOPAEV D.V., MINAKOV P.V., PIROGOV V.G., RAKHIMOV A.T., SUETIN N.V., *Tech. Phys.*, 11 (2007), 1471.
[33] CHILDRES I., JAUREGUI L.A., PARK W., CAO H., CHEN Y.P., *New Dev. Photon Mater. Res.*, 19 (2013), 1.
[34] MAY P.W., LUDLOW W.J., HANNAWAY M., HEARD P.J., SMITH J.A., ROSSER K.N., *Diam. Relat. Mater.*, 2 (2008), 105.
[35] ALMEIDA E.C., TRAVA-AIROLDI V.J., BALDAN M.R., ROSOLEN J.M., FERREIRA N.G., *J. Mater. Sci.*, 7 (2007), 2250.
[36] FERRARI A.C., ROBERTSON J., *Phys. Rev. B*, 20 (2000), 14095.
[37] YAMADA T., KIM J., ISHIHARA M., HASEGAWA M., *J. Phys. Appl. Phys.*, 63001 (2013), 896.
[38] BERNARD M., BARON C., DENEUVILLE A., *Diam. Relat. Mater.*, 4 (2004), 896.
[39] ZIELIŃSKI A., BOGDANOWICZ R., RYL J., BURCZYK L., DAROWICKI K., *Appl. Phys. Lett.*, 13 (2014), 131908.
[40] SOBASZEK M., SIUZDAK K., SKOWROŃSKI Ł., BOGDANOWICZ R., PLUCIŃSKI J., *IOP Conf. Ser. Mater. Sci. Eng.*, 1 (2016), 12024.

Received 2017-05-29
Accepted 2018-04-14